Particles I

Access the latest eBook →

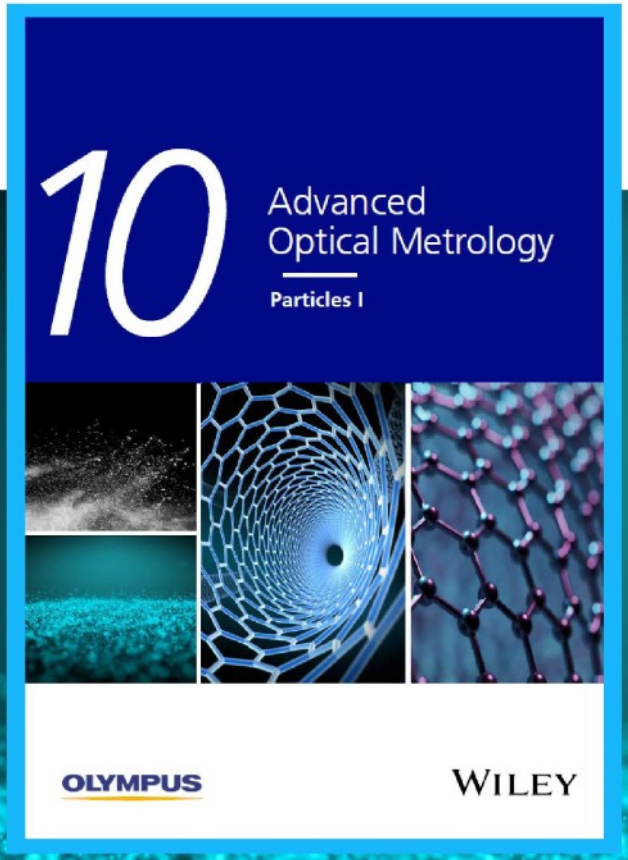

Particles: Unique Properties, Uncountable Applications

Read the latest eBook and better your knowledge with highlights from the recent studies on the design and characterization of micro- and nanoparticles for different application areas.

Access Now

This eBook is sponsored by

OLYMPUS

WILEY

small methods
www.small-methods.com

Protein Ligand Nanopattern Size Selects for Cellular Adhesion via Hemidesmosomes over Focal Adhesions

*Sadegh Ghorbani, Ali Shahrokhtash, Julien E. Gautrot, and Duncan S. Sutherland**

Hemidesmosomes (HDs) are multiprotein complexes that firmly anchor epidermal cells to the basement membrane of skin through the interconnection of the cytoplasmic intermediate filaments with extracellular laminin 332 (Ln332). Considerably less attention has been paid to HDs compared to focal complexes/focal adhesions (FC/FAs) in mechanistic single-cell structures due to the lack of suitable in vitro model systems. Here nanopatterns of Ln332 (100–1000 nm) are created to direct and study the formation of HD in adherent HaCaT cells. It is observed that HaCaT cells at Ln 332 nanopatterns adhere via hemidesmosomes, in stark contrast to cells at homogeneous Ln332 surfaces that adhere via FC/FAs. Clustering of α6 integrin is observed at nanopatterned Ln332 of 300 nm patches and larger. Cells at 500 nm diameter patterns show strong colocalization of α6 integrin with ColXVII or pan-cytokeratin compared to 300 nm/1000 nm indicating a threshold for HD initiation >100 nm but a pattern size selection for maturation of HDs. It is demonstrated that the pattern of Ln332 can determine the cellular selection of adhesion types with a size-dependent initiation and maturation of HDs. The protein nanopatterning approach that is presented provides a new in vitro route to study the role of HDs in cell signaling and function.

1. Introduction

The epidermis is composed of stratified cell layers held together by cell–cell junctions and bound to the basal membrane through cell–extracellular matrix (ECM) adhesions.[1] Epithelial cells attach firmly to the ECM through two types of integrin-containing adhesions termed hemidesmosomes (HDs) and focal complexes/adhesions (FCs/FAs), respectively.[2,3] The existence and form of FCs/FAs as matrix adhesions in vivo is still unclear but well studied in vitro. In the epidermis, cells settled in the basal layer form $\alpha6\beta4$ integrin-mediated HDs structures anchoring the cell membrane to laminin 332 (Ln332) in the underlying extracellular space.[4] While HDs are the major basal layer matrix-adhesion type during homeostatic conditions, a transition from HDs to also utilize FCs/FAs is proposed during wound healing to allow motility and epithelialization of the wound site.[2] Epithelial cells express FC/FA-forming integrins such as $\alpha3\beta1$[5] and readily form FCs in vitro. Induction of motility of cells in the epithelium requires remodeling of both cell–cell and cell–matrix adhesions and is triggered by microenvironmental signals, including mechanical cues and soluble signals (cytokines).[6] The formation and regulation of matrix adhesions and their connection to the cellular cytoskeleton are critical to understand the wound healing processes.

Several proteins play a crucial role in HD formation and a subsequent strong connection to intermediate keratin filaments. These multi-protein junction complexes in (pseudo) stratified epithelia (HDs type I) are composed of specific transmembrane proteins such as $\alpha6\beta4$ integrins, collagen type XVII (so-called ColXVII, BP180, or BPAG2), and two cytoplasmic proteins (plectin and BP230) while simple epithelial (HDs type II) engages only integrin $\alpha6\beta4$ and plectin. Mutations in the structural components of HDs result in different congenital disorders motivating the investigation of these matrix adhesions.[7]

Focal complexes/adhesions are the second type of integrin-comprising cell–matrix adhesion assemblies widely seen in in vitro culture of many cell types.[8] FAs, differently from HDs, connect epithelial cells to the ECM via the actin cytoskeleton. The maturation of FAs from nascent adhesions (FCs) relies upon both intrinsic and extracellular forces, which create cellular tension and occupy an important place in mechanotransduction processes.[9] FCs (containing over six integrins) develop into larger, stabilized FAs with the aid of intracellular adaptor proteins coupled to the actomyosin force machinery.[10,11]

The role of the distribution of ECM integrin-ligands in the formation of FAs has been widely studied via peptide ligands (e.g., RGD) or protein nanopatterns showing both the importance of ligand spacing being below a threshold[12] and the total

S. Ghorbani, A. Shahrokhtash, D. S. Sutherland
Interdisciplinary Nanoscience Center
Aarhus University
Gustav Wieds vej 14, Aarhus C 8000, Denmark
E-mail: duncan@inano.au.dk
S. Ghorbani, A. Shahrokhtash, D. S. Sutherland
The Centre for Cellular Signal Patterns (CellPAT)
Gustav Wieds vej 14, Aarhus C 8000, Denmark
J. E. Gautrot
School of Engineering and Materials Science
Queen Mary
University of London
Mile End Road, London E1 4NS, UK
The ORCID identification number(s) for the author(s) of this article can be found under https://doi.org/10.1002/smtd.202200152.

DOI: 10.1002/smtd.202200152

area[13]/number of ligands.[14–16] We previously reported that the size of vitronectin or fibronectin patches at the nanoscale moderates the transformation of focal complexes into focal adhesions by modulating adapter protein recruitment dynamics and restricting cytoskeletal connection.[13,17]

Recent work has highlighted the interplay between FAs and HDs in epithelial cell motility in wound healing models,[2,3,18] with considerable cross-talk between HDs and FAs, especially during cell migration. Dynamic interaction between the keratin (intermediate filament) and the actin cytoskeleton has been suggested.[18] In other work, Wang et al. identified that HDs play an essential role in signal transduction by the $\alpha 6\beta 4$ integrins and modulate force generation through focal adhesions.[19] The keratin network has been implicated in mechanosensing and cellular response to the surrounding matrix rigidity.[20]

Many studies have been carried out to explore hemidesmosome structure and its effects on cellular behavior in vivo or in vitro among tissues or cell populations. HD plaques in vivo are typically seen with lateral extension in the size range of 200–500 nm via transmission electron microscopy[21] or fluorescence imaging[22] of skin tissue cross sections. In vitro studies with super-resolution microscopy approaches applied to cultured keratinocytes at the single-cell level showed the formation of multiple ≈150 nm clusters of $\beta 4$ integrins localized to intracellular keratins of the intermediate filament network.[22] How the size of hemidesmosomes may be regulated or how they may influence cellular adhesion and function remains an open question. To date, approaches to study HDs have not addressed the role of ligand distribution.

Here, we present a nanopatterned Ln332 platform on transparent substrates to study keratinocyte interactions at model basement membranes which provided a range of ligand patterns (100–1000 nm) to cover from below to above the size of naturally occurring cell–matrix adhesions. The study reveals important events in HD assembly in vitro at a single-cell resolution and correlates to the formation of focal adhesions. Importantly, we show that the Ln332 ligand distribution dictates cellular selection and assembly of hemidesmosomes versus focal adhesions, which implicates ligand distribution as a potential microenvironmental signal for keratinocytes. Nanopatterned ligands provide a tool for isolating HDs for study in vitro.

2. Results and Discussion

2.1. Ti Nanopatterns Fabrication

A systematically varied set of samples composed of different sizes of nanopatterned Ti discs were fabricated via an established colloidal patterning approach[23] coupled with physical vapor deposition. Transparent patterns were formed on 25 mm circular cover glasses enabling integration in normal inverted microscope set-ups. In brief, colloidal nanoparticles were dispersed and immobilized onto glass samples precoated with a polymer resist through electrostatic self-assembly. A so-called sacrificial hole mask was formed by the removal of colloidal particles after evaporation of a thin Ti film and subsequent oxygen plasma etching. The hole masks were then utilized to form Ti discs that could define protein nanopatterns (**Figures 1**; Figure S1a, Supporting Information). The diameter of Ti discs could be specified by the colloidal particle size selected for the process in the range of 100–1000 nm. The nanopatterns were then characterized by SEM and atomic force microscopy (AFM). SEM was carried out on the samples fabricated via the colloidal lithography process before protein attachment to check the monodispersity and pattern quality of the nanosized Ti discs (**Figure 2**a). Characterization data for nanopattern patch size, polydispersity, and total area coverage are shown in the supplementary information (Table S1, Supporting Information). To prevent possible mechanotransduction signaling effects from the topography of the nanopatterned disc itself, only 2 nm Ti was deposited. When oxidized, their height is raised to approximately 4.5 nm, measured using AFM (Figure S1b, Supporting Information) comparable to the hydrated protein rejecting polymer layer used to coat the silica background.

2.2. Ln332 Protein Patterning

The glass samples were incubated with DDP (dodecyl-phosphate ammonium salt) overnight to preferentially functionalize the TiO_2[24] and provide a chemical contrast between the hydrophilic SiO_2 and the hydrophobic functionalized discs allowing site-specific immobilization of Ln332 protein on top of the discs. The PLL-g-PEG gives the SiO_2 background a robust antifouling character,[25] while the hydrophobic DDP chemistry prevented the PLL-*g*-PEG from forming on the disc regions and allowed subsequent biomolecule adsorption. PLL-g-PEG at micropatterned SiO2 and DPP/TiO2 patterns could limit cell interaction to the DPP/TiO2 regions for at least 14 days.[26] ECM proteins including laminins can bind non-specifically but irreversibly into a nanopattern and retain their function.[13,27] Immunofluorescent staining demonstrated that the Ln332 protein nanopatterns were successfully assembled for all desired sizes (Figure 2b). Fluorescence Ln332 protein patterns show the protein was restricted to circular colloidal lithography-generated Ti domains with a well-controlled size. The discernible patch areas compared to the background seen in Figure 2c show negligible background protein attachment on the passivated PLL-g-PEG regions (>97% has been reported as the passivating efficiency of PLL-g-PEG[28]). The 300 nm discs are close in size to the resolution of our microscope; however, the fluorescent image demonstrates a distinguishable Ln332 pattern. To resolve the 100 nm diameter patterns, which are below the diffraction limit of traditional fluorescence microscopes, we applied a super-resolution technique, DNA-PAINT imaging.[29] Figure 2b shows high-intensity 100 nm domains, which indicates the successful development of Ln332 patterns.

2.3. Cell Morphology

The ability of cells to adhere to the different ligand patterns was first assessed at the cell level. The attachment, growth, and spreading of an epithelial cell line, HaCaT, onto the Ln332 nanopatterns with a systematically varied size was qualitatively investigated after 12 h and compared to homogeneous Ln332 surfaces (**Figure 3**a,b).

Figure 3c shows representative fluorescence micrographs of HaCaT cells adhering to homogeneous substrates and 100, 300,

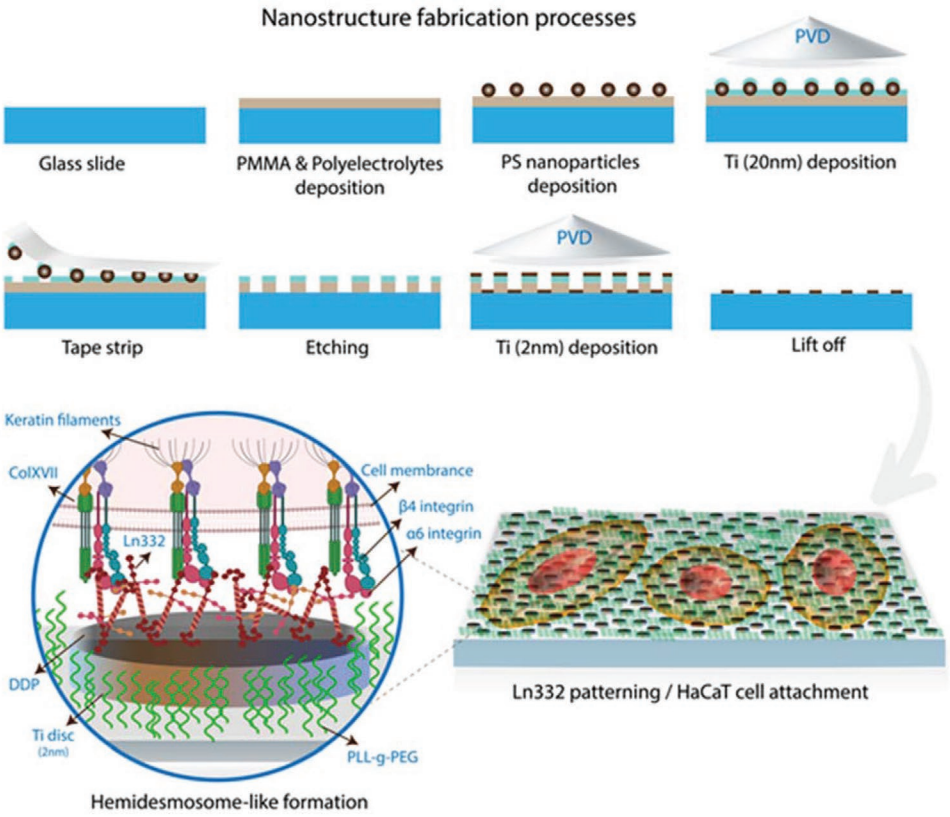

Figure 1. Schematic shows the procedures for the Ln332 nanopatterning using hole mask colloidal lithography via nanoparticle deposition on a glass slide followed by mask creation and Ti deposition to develop a nanosized TiO_2/SiO_2 pattern. Samples were incubated with DDP functionalizing the TiO_2 to create a chemical contrast followed by PLL-g-PEG deposition and Ln332 deposition. The zoomed-in region represents the hemidesmosome-like formation of HaCaT cells on Ln332 patches through the attachment of specific proteins to keratin filaments.

500, 1000 nm Ln332 patterns. The attachment efficiency of HaCaT cells after 12 h for the negative control (PLL-g-PEG) was below 5% (Figure S2c, Supporting Information), which is in accordance with other detailed studies of cells on similar surfaces.[30,31]

Quantified data of cell attachment from one repeat is shown in Figure 3e with all repeats shown in Figure S2a (Supporting Information). All ligand-containing surfaces showed a high seeding efficiency (close to 100%) although with a lower level for the smallest pattern size across the three repeated experiments ($n = 3$). No significant difference in cell attachment among individual sizes of nanopatterned Ln332 was found, which suggests that the size of the protein patch has no meaningful impact on the cell seeding efficiency (Figures 3e; Figure S2, Supporting Information). At the cell seeding densities used, most cells were present as single cells after 12 h, and cell areas and circularities could be characterized (Figures 3c,d). The cells on the homogeneous Ln332 are well spread with a significantly larger area (approximately a factor of 3) and a more clearly defined actin cytoskeleton compared to the nanopatterned ligands. The nanopatterned surfaces were overall similar and showed a range of cell areas and shapes (judged by circularity), including essentially unspread cells, moderately spread cells, and cells with a stellate appearance with cellular membrane protrusions and lower circularity. The whole-cell population data showed small differences in the average spread areas and average circularities for different pattern sizes (Figures 3c,d). Cell shape classification based on size and circularity was carried out and is shown in Table S2 (Supporting Information) correlating to the differences in average cell area and cell circularity. The cells at the nanopatterns showed stable attachment but less defined cytoskeletons, smaller size, and a larger fraction of unspread and stellate cells than the homogeneous ligand presentation but with no strong differences at the cell level seen for different ligand pattern sizes. Overall, these data indicate that Ln332 circular nanopatterns restrict HaCaT adhesion, cytoskeleton assembly, and spreading, compared to homogenous substrates, at all laminin adhesive patch sizes tested.

2.4. Cellular Adhesion Processes

Epidermal cells can adhere to Ln332 through two different integrin-mediated mechanisms, via focal contacts/adhesions linking to the actin cytoskeleton and/or through hemidesmosomes linking to the keratin network. To shed more light on the adhesion mechanisms occurring at the different ligand presenting interfaces, we applied higher magnification confocal fluorescence microscopy (×63 or ×100) to identify proteins involved in FCs/FAs or HDs, respectively. Cells were co-stained with the HD-associated proteins (α6 integrin, ColXVII, and pan-cytokeratin) or the FC/FA-associated protein vinculin and the actin cytoskeleton. The unpatterned substrates showed

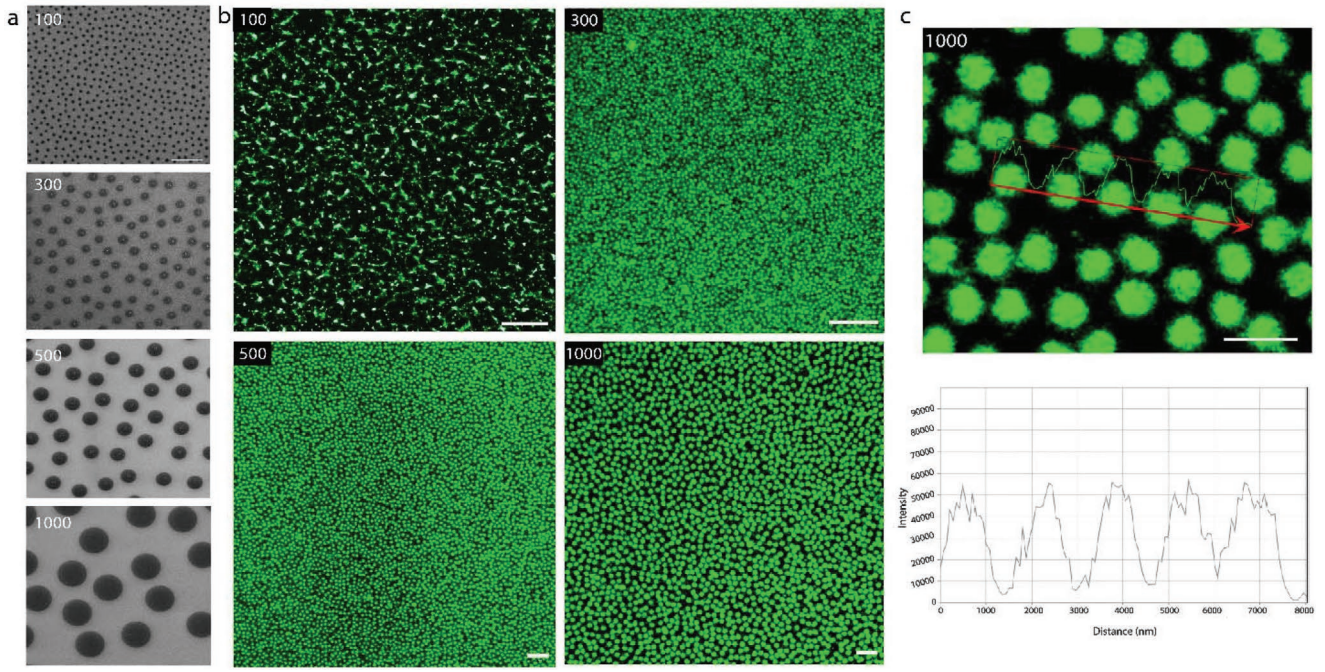

Figure 2. Characterization of the nanopatterned structures. a) SEM images of the different-sized Ti nanopatterns (100–1000 nm) without polymer/protein modification. Scale bar = 1 µm. b) Immunofluorescence staining of Ln332 protein illustrates the protein nanopatterns for 100–1000 nm patch sizes. The DNA-PAINT image (top left panel b) represents 100 nm protein patterns (scale bar, 2 µm). Confocal microscopy images illustrate other Ln332 patch sizes (300–1000 nm; scale bar, 5 µm). c) Zoom of protein pattern and trace of the intensity of stained protein patterns (1000 nm) with Ln332 antibody, along the drawn line, Scale bar = 2 µm.

that the cells grown on homogeneous distributions of Ln332 exhibit strong staining for FC/FA-associated proteins but weak staining for HDs associated proteins (**Figure 4**a,b). It has previously been shown that HD and FA complexes localize in adjacent regions when cultured on uncoated tissue culture wells in serum, which proposes their cooperation in traction force regulation.[18] Based on the obtained fluorescence images and colocalization of well-defined actin stress fibers (stained with phalloidin) with vinculin stained domains, HaCaTs mainly utilize FAs to attach to the homogeneous Ln332 surface rather than HDs. The adhesion appears to be via engagement of actin coupled to FCs/FAs (Figure 4c and Figure S3a, Supporting Information). Neither α6 integrin nor ColXVII was apparently recruited or clustered at the basal cell membrane, and these proteins do not appear to be involved in the adhesion processes, with very few examples of visible links to the intermediate keratin filament systems (stained with pan-cytokeratin) (Figure S3a, Supporting Information).

In contrast, cells adhering to the nanopatterned surfaces showed little evidence of focal adhesions, and while cortical actin and/or transverse actin networks were clearly seen in cells adhering to these substrates, few dorsal actin fibers were seen (connecting the transverse fibers to FAs and the material surface; **Figure 5**). Cellular assembly of HDs was clearly observed at the larger pattern sizes but in a ligand patch size-dependent manner. The 500 nm diameter patterns showed assembly of mature HDs with strong colocalization of integrin α6 with the Ln332 patterns indicating the formation of an integrin-based adhesion. HD assembly was confirmed by colocalization of ColXVII in the adhesions and maturation of the HDs by colocalization of the HDs with focal points of keratins in the basal plane of the cells visualized through pan-cytokeratin staining (**Figures 6;** Figure S5, Supporting Information). The expression of α6 integrin and pan-cytokeratin (Pan cyto) at the same position reveals that the formed HDs structures were mature enough to be connected to the cytoplasmic keratin filament network and provide strong adhesion.[32] Of particular note, we observed these large assembled protein patches representing HD formation only at the interface of the cells and the substrates, with only isolated proteins/small protein clusters randomly distributed all over the cytoplasm/membrane at higher sections (Movies S1 and S2, Supporting Information).

At an earlier time point (2 h) cells were attached to the patterned surfaces, however, the expression level of α6 integrin was relatively weak. The first circular patches of α6 integrin appeared after 3 h post cell seeding, and matched the size of Ln332 patterns (e.g., 500 nm, Figure S4, Supporting Information). The patterns of expressed α6 integrin at the bottom section of cells at the interface to Ln332 patches were observed on both single cell and the cell population for 12 and 24 h (500 nm, Figure S4, Supporting Information). Overall, these results indicate that HaCaTs spreading on 500 nm Ln332 patterns utilized mature HDs to bind to the surface. Smaller pattern sizes, while supporting adhesion of cells did not appear to effectively form mature HDs. Cells at 100 nm diameter patterns showed consistent but relatively low expression of α6 at the interface with the substrate with no clearly defined localizations. There was no indication of recruitment of ColVXII or connection to the keratin network, indicating that 100 nm Ln332 patches do not allow assembly of HD adhesions.

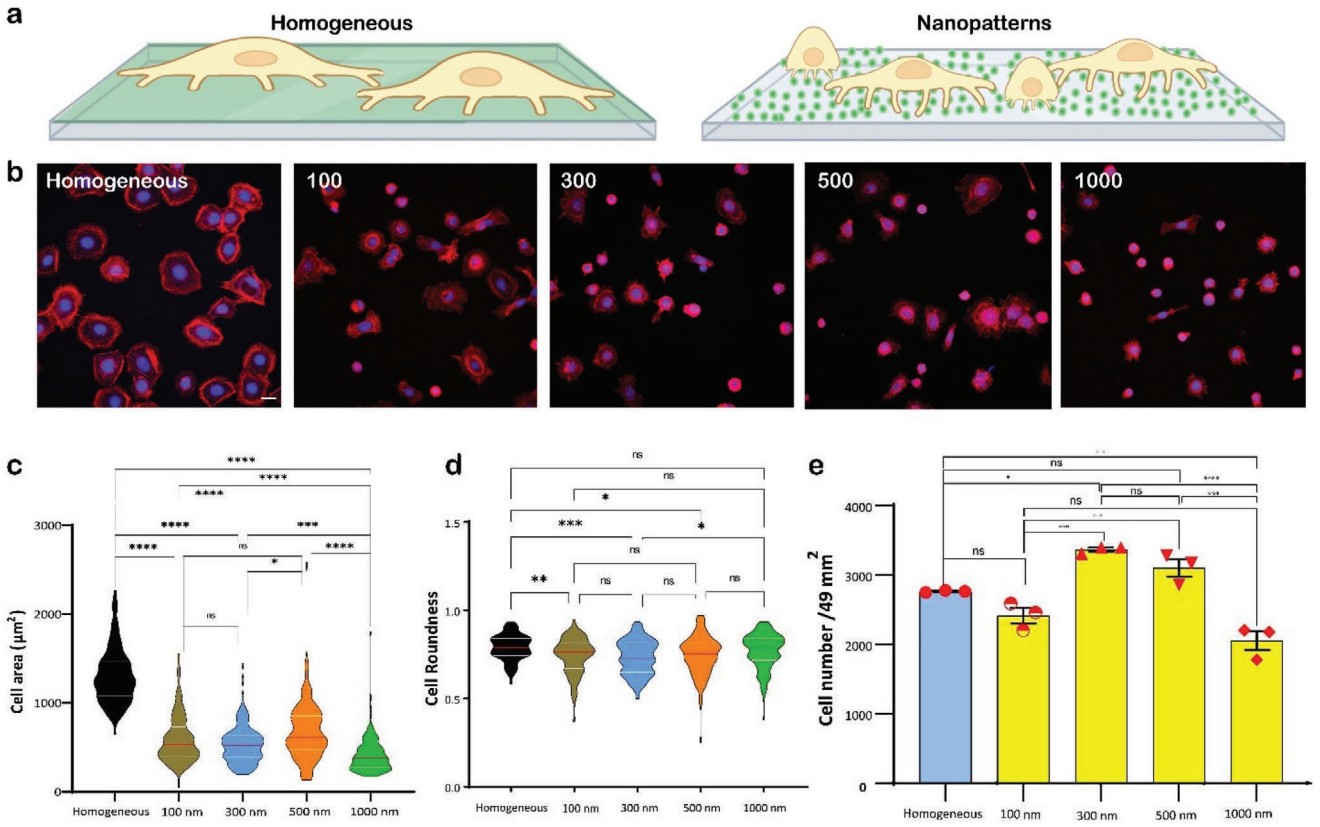

Figure 3. Nanoscale restriction of Ln332 controls HaCaT cell spreading in a size-independent manner, but not cell attachment efficiency. a) Schematic representation of cells spreading on nanopatterns indicating approximate relative sizes. c) Distribution of cell areas, d) distribution of cell roundness, e) Attached cell numbers per well (49 mm^2) (measured 12 h after cell seeding on the substrates for one repeat). b) representative immunofluorescence microscopy images of HaCaT spreading on homogeneous Ln332 or 100, 300, 500, or 1000 nm nanopatterns of Ln332 (DAPI, blue; F-actin/phalloidin, red). Scale bar = 20 μm, c) distribution of cell areas, d) distribution of cell roundness, e) attached cell numbers per well (49 mm^2) measured 12 h after cell seeding on the substrates for one repeat. The data are acquired from six images per sample and three samples per condition. Significant differences between each sample are displayed by (*<0.1,**<0.01,***<0.001, ***<0.0001), while non-significant differences are shown by (ns).

Interestingly, recent super-resolution characterization showed integrin clusters of ≈150 nm, and the lack of clustering here could indicate that 100 nm patches cannot support sufficient integrin to initiate HD assembly. It is likely that 100 nm patches of ECM proteins cannot support more than a few integrins (≈3) because of geometric constraints.[31] Cellular adhesion to the surface is likely through individual or small clusters of integrins without the formation of HDs of FC/FAs or a strong connection to the cytosolic cellular skeletal proteins. Cells at the 300, 500, and 1000 nm diameter patterns show clear α6 integrin colocalized with the Ln332 nanopatterns (Figures S7 and S8, Supporting Information). However, in contrast to cells at 500 nm diameter patterns, the smaller and larger pattern sizes showed only weak colocalization of the α6 with ColXVII or the keratin network (Figure 6a,b; Figure S5, Supporting Information) that indicates that although the 300 and 1000 nm diameter patterns can lead to localization of the α6 integrin at the membrane into clusters through binding to the Ln332, these assemblies are poorly able to mature the complex by recruiting adaptor proteins and form a connection to keratin network. It should be noted that cells at the 1000 nm diameter patterns showed some signs of abnormal appearance (e.g., the bleb-like structures seen in the 1000 nm-vinculin stained image in Figure 5). We cultured the cells longer to clarify the health of the cells in this serum-free media and imaged them after 24 h. Interestingly, while cells at the homogeneous, 100, 300, and 500 nm diameter patterns of ligand distributions after 24 h showed similar morphologies/adhesions to 12 h, the cells at the 1000 nm diameter patterns displayed different morphologies. We consistently observed cells with substantially reduced size and retracted membrane and appears to have left behind the membrane and cytosolic components at these 1000 nm patches after 24 h (Figures S8 and S9, Supporting Information), suggesting that 1000 nm diameter patterns of Ln332 are not able to support long term culture in these serum-free conditions. In this work, we observe that keratinocytes switch their adhesion process from FAs to HDs by spatially restricting the ligand availability but we also observed a selective ability of surfaces to induce the formation of α6 clusters or to mature HDs and connect to the keratin network based on the lateral dimensions of Ln332 patterns.

In previous work, we have shown that the size of FC/FAs can be restricted by the size of a ligand patch for several other cell types using the ECM proteins fibronectin or vitronectin.[17,31]

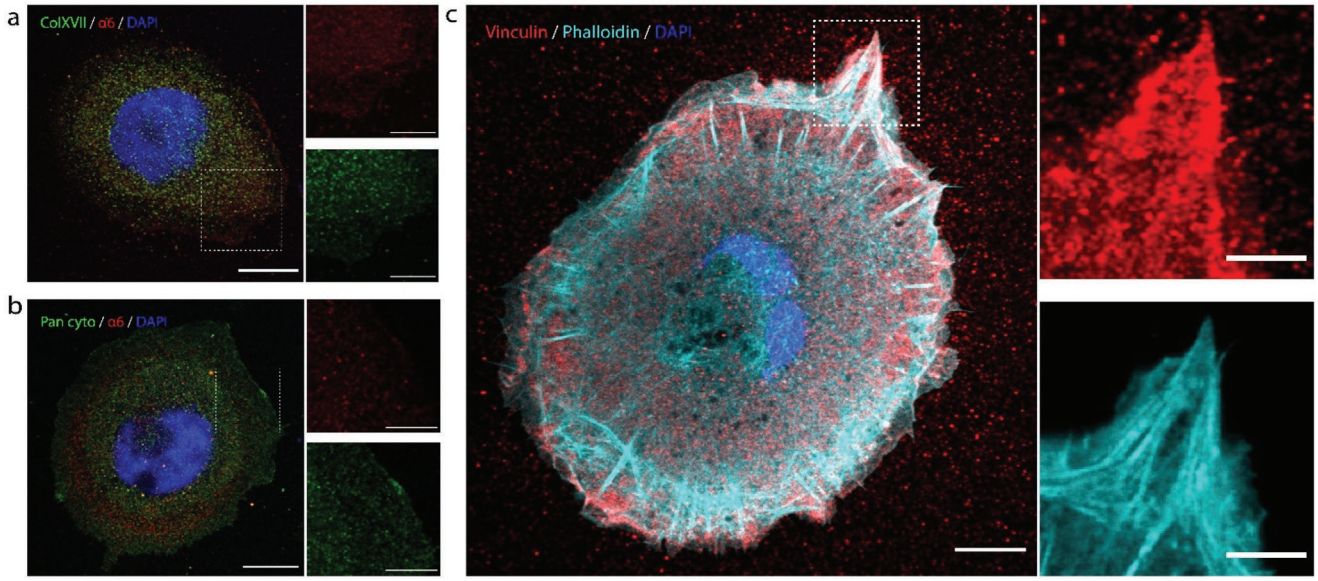

Figure 4. CLSM images of HaCaT cells on Ln332-coated homogeneous surface. Panels (a) and (b) demonstrate low expression of α6 integrin, pan-cytokeratin, and ColXVII proteins on homogeneous Ln332 samples. In CLSM images, no significant localization of α6 integrin with pan-cytokeratin (Pan cyto) and ColXVII proteins inside the cells was observed. Panel (c) illustrates that cells express vinculin that co-localizes with the tip of actin stress fibers (stained with phalloidin in cyan), suggesting mature focal adhesions formed in those regions. The CLSM analysis was repeated three times independently with similar results. Scale bars = 10 µm, inserts = 2 µm.

Here, we checked our system of protein patterns by comparing the adhesion of another cell type that cannot form HDs (fibroblasts) to Ln332 and HaCaTs to another ligand (fibronectin) that does not support HDs. Fibroblasts were cultured on 500 nm Ln332 patterns for 12 h. Generally, fibroblasts are one of the cell populations in the skin, which cannot form HD because they lack α6 and β4 integrins.[33,34] The absence of plectin (a common protein in both HDs and FAs) in fibroblasts has been correlated with an amplified number of actin filaments and FAs formation.[24] Our results also showed that the cells expressed higher vinculin levels (FAs assembly) but, as expected, did not assemble HD structures (Figure S6a, Supporting Information). HaCaTs were cultured on 500 nm ligand patterns of fibronectin to explore if they could adhere to similar pattern sizes through FC/FAs. The cells showed attachment but did not colocalize HD proteins (α6 or ColXVII) at the FN ligand patterns but localized vinculin indicating adhesion through FC/FAs (Figure S6b, Supporting Information). The images suggested that the α6 was excluded from the ligand patches likely by one of the ranges of fibronectin-binding integrins including $\alpha5\beta1$, $\alpha v\beta1$, and $\alpha v\beta6$ that HaCaTs express.[35] In our system, we prepare a protein-ligand pattern, but it is clear that cells may secrete their own ECM in a few hours.[36] In a previous study of epidermal stem cells cultured at fibronectin patterns of different sizes, we observed the deposition of cellular laminin and the formation of HDs but always together with FC/FAs.[17] Our results here at 500 nm ligand patterns indicated that any secreted laminin could not outcompete the immobilized FN (Figure S6b, Supporting Information). These data are in line with the observation that any disorganization of the communication between $\alpha6\beta4$ integrins and intermediate filament systems (keratins) or Ln332 leads to more mature focal adhesion development.[19] The nanopatterns we prepare provide Ln332 either homogeneously (100% coverage) or distributed within nanopatterns with lower coverage. The distance between patterns and the overall coverage of ligand varies to some extent as the patch sizes are changed. While the difference in coverage and thus the total amount of available ligand between the homogenous versus nanopatterned surface (>factor of 3) may play some role when comparing homogeneous and nanopatterned surfaces, the difference between coverages of nanopatterns is much less (e.g., 300 nm/500 nm diameter patterns have coverage of 19.9%/21.8% respectively). The distance between the patches varies (200–400 nm) considerably across a region encountered by a single cell and also between samples of different patch sizes as a result of our fabrication process but maintains a minimum characteristic spacing of above 200 nm (edge to edge). This distance appears to be large enough to prevent bridging between ligand patches by a single HD as has been observed for other adhesion types.[13,37,38] We believe that the patch size is the dominating factor in determining cellular response.

We utilized electron microscopy to observe the cellular interactions with the surfaces at higher magnifications, and attached cells were fixed after 12 h and examined with SEM. All the ligand pattern sizes showed that the outer edge of the cell membranes showed clear protrusions correlated to the ligand patterns confirming the adhesiveness of the ligand patches and the antifouling properties of the background (PLL-g-PEG). Cells attaching to the homogeneous ligand substrates also showed membrane extensions but with large width and signs of localized adhesions (**Figure 7**). Most membrane extensions from cells at the nanopatterned surfaces are sequentially connected to several Ln332 patches.

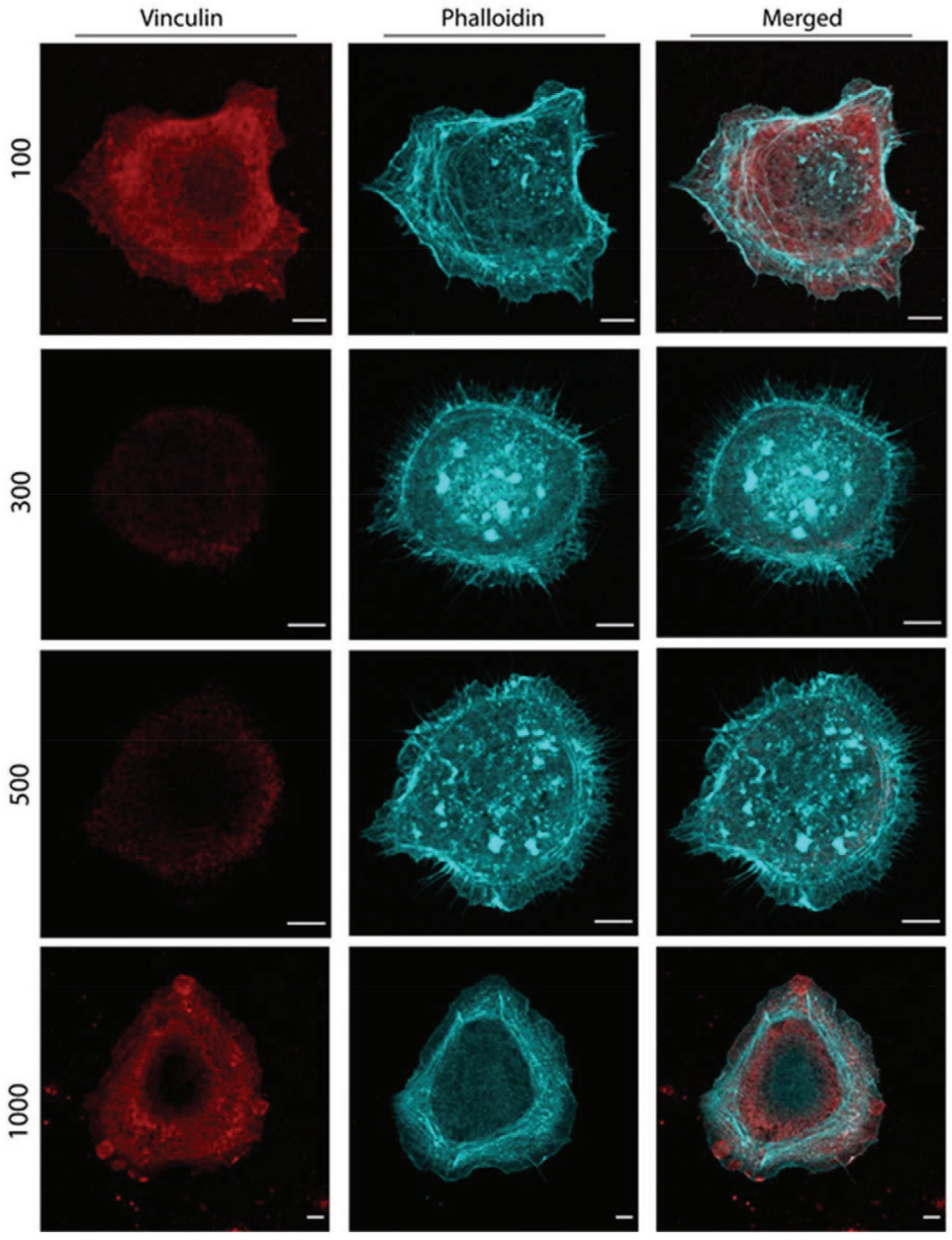

Figure 5. CLSM images of HaCaT cells on homogenous and nanopatterned Ln332 structures after 12 h seeding. Images represent weak vinculin (in red) expression levels for 300 and 500 nm groups where cells formed cortical actin (in cyan) structures, Scale bar = 5 µm.

We have observed a different behavior of keratinocytes at substrates displaying the ECM cell adhesion ligand Ln332 either as a homogeneous distribution or nanopatterned into discrete patches or different sizes. The first clear result is that by restricting the distribution of Ln332 to nanopatterns the keratinocytes no longer significantly formed focal adhesions. At the homogeneous ligand distribution, we observed both low expression of $\alpha 6$ integrin and no clear localization, and clear evidence of vinculin-stained focal adhesions linked to the actin cytoskeleton. Cellular attachment at the homogeneous ligand distributions is likely via $\alpha 3\beta 1$ that has been shown to be critical for epidermal stem cell migration on Ln332.[39] At nanopatterned Ln332, the formation of FCs appears to be disrupted and we conjecture that this relates to there being too few integrins engaged in the ligand patches to support the maturation of FCs as has been seen previously for cells adhering to fibronectin and vitronectin nanopatterns.[13] The lack of focal adhesion formation in our system leads to a switch toward the formation and maturation of HDs and we observed a threshold for ligand patch size to allow clustering of the $\alpha 6$ integrin at 300 nm. However, we do not observe clear maturation of the HDs in terms of recruitment of COLXVII and connection to the cytoskeleton until a threshold of 500 nm, suggesting by geometric consideration the need for $>\approx 60$ $\alpha 6$ integrins for

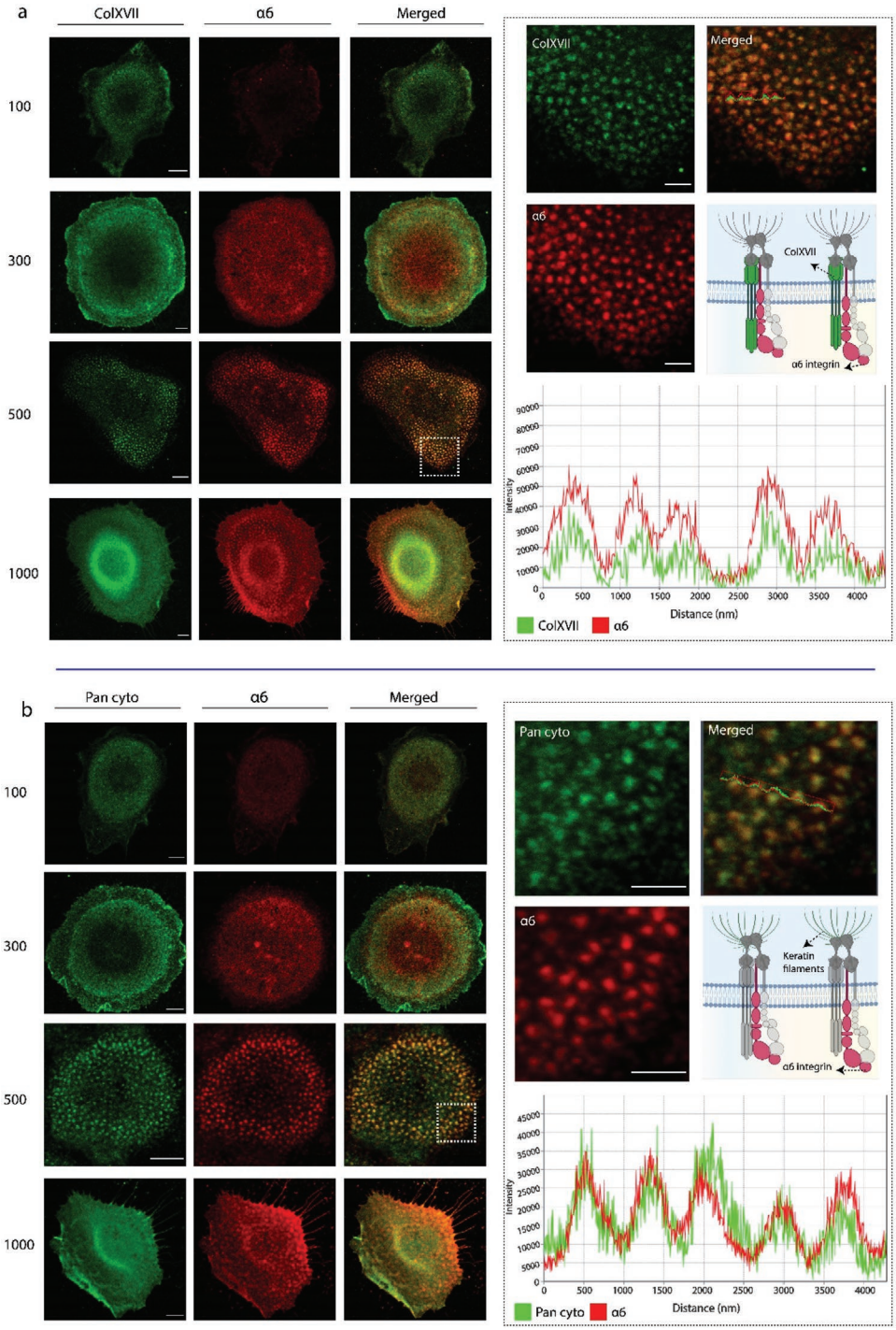

Figure 6. CLSM images of HaCaT cells on Ln332 nanopatterns after 12 h post culture. Panel (a) represents colocalization of ColXVII and α6 integrin. Panel (b) shows colocalization of pan-cytokeratin and α6 integrin, Scale bars = 5 µm.

assembly.[31] At 1000 nm ligand patterns, we observe only α6 integrin clustering and weak HD maturation and cells appear to not be able to survive long term. These results indicate that the size of Ln332 ligand patterns can determine the cellular adhesion mechanism and suggests ligand distribution may be an important environmental signal in wound healing and a potential bioengineering route to steer cell behavior.

3. Conclusion

Here, we demonstrate that ligand nanopatterns of Ln332 can steer keratinocytes (HaCaT) to adhere via hemidesmosomes/keratin network rather than via focal adhesions/actin cytoskeleton while cells at homogeneous Ln332 predominantly adhere through focal adhesions. Our patterning approach enables

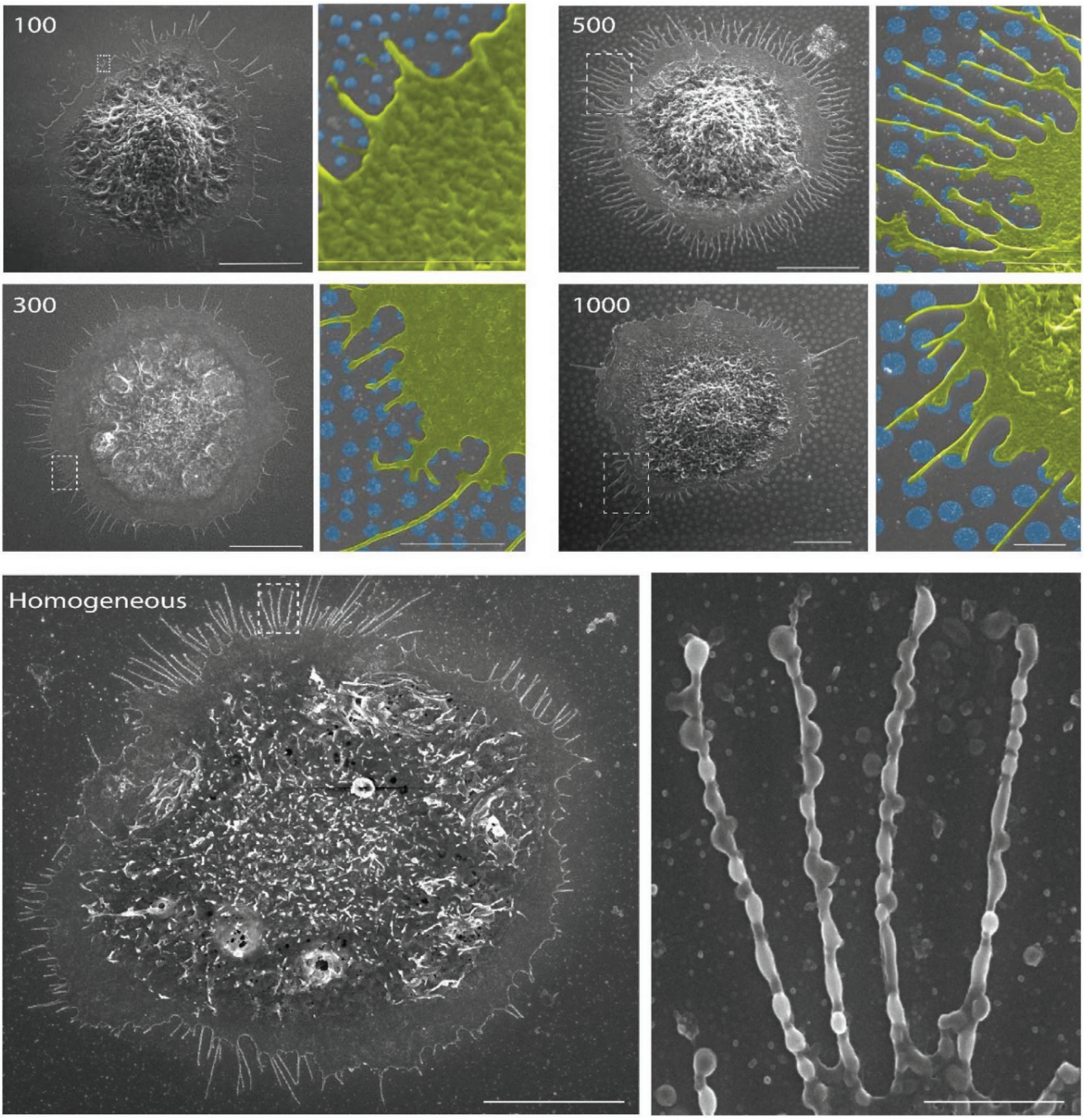

Figure 7. SEM images of attached HaCaT cells on homogeneous and nanopatterned Ln332 structures after 12 h post culture. Scale bars = 10 µm, Inserts = 5 µm.

control of protein patterns over the size range of 100–1000 nm on a transparent format over large areas. The methodology enables the selection of a specific adhesion type in an in vitro format enabling studies of HD assembly. Interestingly, we observe a threshold of ligand pattern size for assembly of HDs above 300 nm and a size selection for clear maturation and connections of the HDs to the keratin network at 500 nm. This work gives insight into the role of ligand distribution at the nanoscale on cellular adhesions to basal laminin. The use of nanopatterns to externally control HD assembly has the potential for use in mechanistic studies exploring signaling of this adhesion type and the role of HDs in motility and wound healing. In this context of skin biology, this in vitro HD model system could be used to shed more light on the sensing mechanisms of epidermal stem cells at the nanoscale and investigate the role of HD formation on stem cell fate determination via high throughput imaging approaches. Understanding these mechanisms will assist the design of

engineered platforms and state-of-the-art materials for regenerative medicine applications.

4. Experimental Section

Materials and Reagents: PDDA (poly(diallyldimethylammonium chloride)), PSS (poly(sodium-4-styrenesulfonate)), and PEI (polyethylenimine, branched) were purchased from Sigma–Aldrich (DK). Polystyrene colloidal particles, sulfate latex diameters 100, 300, 500, and 1000 nm were obtained from Invitrogen (US). Laminin 332 was purchased from Biolamina (SE). Fibronectin from human plasma was from R&D system. Fetal bovine serum (FBS) was obtained from Invitrogen (US). Moreover, a Synergy system from Millipore was used to produce deionized water.

Fabrication of Nanostructured Surfaces: Hole Mask Colloidal Lithography (HMCL)[23] was used to prepare transparent chemical nanopatterns of TiO_2/SiO_2 on glass substrates.

Substrate Cleaning and Resist Spinning: Glass slide substrates (#1.5) (Menzel, DE) were cleaned by sonication in acetone followed by isopropanol. The substrates were then treated with oxygen plasma (Advanced Vacuum RIE system, Vision 300 MKII, Plasma-Therm, US, O_2 pressure = 25 mTorr, power = 100 W, flow rate = 40 sccm) for 10 min to remove any remaining organic contamination. The cleaned glass substrates were baked on a hot plate at 200 °C for 10 min to dehydrate the substrate. Afterward, 4% PMMA solution (Mw = 495K in Anisole, Microchem, US) was added to the substrate and spin-coated at 3000 rpm for 60 s, followed by baking on a hotplate at 180 °C for 2 min.

Polyelectrolyte and Particle Deposition: Three different polyelectrolytes were sequentially deposited onto samples. First, 2 wt.% PEI solution (Mw ≈25 000) in deionized water (DI water) was loaded on the sample for 30 s, followed by rinsing with DI water for 1 min and drying with a nitrogen gun. This procedure was repeated using 2 wt.% PSS solution (Mw ≈70 000) and 0.5 wt.% PDDA solution (average Mw 200 000–350 000) in DI water, respectively. Polystyrene nanoparticle solution of 100 nm (actual size: 120 nm), 300 nm (actual size: 320 nm), 500 nm (actual size 470 nm), and 1000 nm (actual size 990 nm) (Invitrogen Molecular Probes, Thermo Fisher, USA) with the concentration of 0.2 wt.% in DI water was then loaded onto the samples for 15–60 min and rinsed with DI water for 1 min. The nanoparticle-coated substrates larger than 100 nm were transferred into sealable heating chambers filled with boiling water and baked in an oven at 120 °C for 20 min to protect the particle pattern against capillary-induced aggregation during drying.[13] Then, the samples were taken out of the water and dried carefully under nitrogen flow.

To prepare the hole mask, a titanium mask (20 nm) layer was deposited by e-beam evaporation (Cryofox explorer 400 GLAD, Polyteknik, $<10^{-7}$ Torr, DK), and the nanoparticles were stripped off with tape. Subsequently, reactive ion etching O_2 = 25 mTorr, power = 50 W, flow rate = 40 sccm, time = 10 min) was applied to etch the PMMA layer to create cavities used as the write-field in HMCL. The deposition of the final nanostructures for all patch sizes was then carried out by depositing 2 nm titanium. All depositions steps (including the mask) were performed at a constant speed mode. The deposition rate during film formation was controlled by an in situ quartz crystal microbalance allowing control of average film thickness within ≈0.1 nm. The rotation was 3 rpm, deposition angle 0° (i.e., perpendicular to the substrate plane), deposition rate 0.5 Å s^{-1}. In the end, the sacrificial layers were removed by 1 min sonication in acetone, isopropanol, and DI water, respectively.

Protein Immobilization on Nanopatterned Surfaces: The deposited Ti discs were first completely oxidized via RIE (O_2 pressure = 25 mTorr, power = 75 W, flow rate = 40 sccm) for 2 min and then were incubated with 0.5×10^{-3} M DDP (dodecyl-phosphate ammonium salt) at room temperature overnight.[40,41] The combination of TiO_2/SiO_2 and DDP was previously reported for protein nanopatterning to assemble lipid vesicle arrays.[24] Subsequently, samples were washed three times with deionized water for 2 min and dried under nitrogen flow. The protein rejecting background was formed by poly(L-lysine)-g-poly(ethylene glycol) PLL(20)-g[3.5]-PEG(2)[25] (Surface solutions, CH, 250 µg mL^{-1} in 10×10^{-3} M HEPES pH 7.4) that was loaded on the samples for 1 h at room temperature and then were rinsed by PBS 3 times (1 min per each step). Next, laminin 332 (Ln332, 5 µg mL^{-1} in PBS) was incubated on each sample overnight at room temperature and then was washed by PBS as described earlier. The transparent homogenous and patterned Ln332 (100, 300, 500, 1000 nm) structures were then utilized immediately for cell studies.

Cell Experiments—Cell Culture and Seeding: HaCaT cells were cultured in high glucose Dulbecco's modified Eagle's medium (DMEM) supplemented with 100 IU mL^{-1} penicillin, 100 µg mL^{-1} streptomycin, and 10% fetal bovine serum (FBS) until reaching 70% confluency. The samples for cell experiments were plasma treated right before the functionalization and were then mounted onto the 16-well chambers (ProPlate multi-well chambers, Grace bio-labs, US). Cells were then detached and seeded on the samples at a density of 3000 cells per well (49 mm^2) and incubated in DMEM without FBS for 12 or 24 h in a humidified 37 °C, 5% CO_2 incubator.

Fibroblast cells were cultured at the same condition in DMEM/10% calf fetal bovine serum.

Characterization/Imaging—Immunostaining, Antibodies: For immunofluorescence, cells were fixed with 4% paraformaldehyde for 30 min, permeabilized with Triton-X-100 (0.2%) (Thermo Fisher, US) for 10 min, and blocked with 10% goat serum for 15 min. Primary antibodies were added and incubated overnight at 4 °C. The samples were washed with PBS-T (PBS-Tween 20) and then conjugated with secondary antibodies for 1 h at room temperature. DAPI (4,6-diamidino-2-phenylindole) was added to the secondary antibody solution for nucleus staining, and the samples were mounted on a glass slide with ProLong Glass Antifade (Thermo Fisher, US).

Cells on Ln332 nanopatterns or PLL-g-PEG controls without Ln332 were analyzed. The imaging was carried out using a confocal laser scanning microscope (CLSM, LSM 700, Zeiss, DE) with 40× 0.5 NA, 63 × 1.2 NA, and 100 × 1.5 NA oil lens systems. The images were then processed by the software ImageJ.[42]

The mouse anti-ColXVII (1:200, ab186415) and rat anti-6 integrin (1:1000, clone GoH3, ab105669) were purchased from Abcam. The mouse anti-pan cytokeratin (1:200, MA1-82041) was purchased from Thermofisher, and mouse anti-laminin 332 (1:200, sc-13587) was obtained from Santa Cruz. The mouse anti-vinculin (1:800, V9131), TRITC-phalloidin (1:500, P1951), and DAPI (1:1000, 28718-90-3) were from Sigma Aldrich.

DNA PAINT: An Oxford Nanoimager S in TIRF mode was used for DNA-PAINT super-resolution imaging. For DNA PAINT imaging, DBCO-terminated 7xR3 SPEED-PAINT docking strands[43] (IDT, US) were conjugated to the azide modified goat anti-mouse IgG H&L preadsorbed (ab7063, Abcam, UK) and purified by an MWCO 100 kDa Amicon filter. The 100 nm ln332 nanopatterns were revealed by immunostaining with mouse anti-laminin 332 (1:200, sc-13587) for 2 h. Subsequently, the 7xR3 docking strand conjugated anti-mouse IgG was incubated for 1 h at 1:1000 on the surface.

For imaging, Cy3B-conjugated R3i/7 nt imager at 50×10^{-12} M in imaging buffer C+ (PBS + 500×10^{-3} M NaCl & 0.05% Tween-20) with the addition of oxygen scavengers, according to the published protocol by Strauss et al. was used. A 561 nm laser illuminated the sample with a power density of ≈2.5 kW cm^{-2}.

A total of 10 000 frames with an exposure time of 100 ms were taken, and the images were drift corrected using 90 nm Au fiducial markers and reconstructed in Picasso.[29,43]

Scanning Electron Microscopy: Image acquisition was carried out using Magellan 400 SEM (FEI, US) with acceleration voltages ranging from 1 to 5 kV and currents ranging from 25 to 100 pA.

SEM was used to image samples with the attached cells on the surfaces. Cells were first fixed with 2.5% Glutaraldehyde for 30 min at room temperature. Next, cells were dehydrated in a graded series of ethanol (30%, 50%, 70%, 85%, 95%, and 2 × 100%) for 30 min each.

Dehydrated samples were dried under a stream of nitrogen. A 10 nm Ti layer was deposited on the samples via physical vapor deposition for conductivity, and the samples were imaged by SEM.

Atomic Force Microscopy: The imaging was done using Dimension Edge AFM (Bruker, USA) in tapping mode (RTESP-300, Bruker, USA). The structures were imaged on the day they were fabricated. The ratio between the free amplitude and the contact amplitude setpoint was kept at ≈0.6. The height images were generated on the software, Gwyddion.[44]

Statistics: The statistical analysis was performed using GraphPad Prism version 9.1. The cell number data were analyzed statically by two-factor ANOVA and Tukey's test for post hoc analysis. Moreover, the cell area and roundness data were analyzed by the Kruskal–Wallis test. Significant differences were only indicated for each data point compared to the homogenous surfaces for Ln332 or among the different sizes of protein patterns. The sample size was included in the legend of each figure. Quantitative data were presented as mean ± standard error.

Supporting Information

Supporting Information is available from the Wiley Online Library or from the author.

Acknowledgements

This work acknowledges funding from the Danish National Research Foundation center grant CellPAT (DNRF135) (S.G., A.S., and D.S.S.).

Conflict of Interest

The authors declare no conflict of interest.

Data Availability Statement

The data that support the findings of this study are available from the corresponding author upon reasonable request.

Keywords

laminin 332, focal adhesions, hemidesmosomes, protein patterning

Received: February 2, 2022
Revised: March 15, 2022
Published online:

[1] F. M. Watt, *Science* **2014**, *346*, 937.
[2] S. B. Hopkinson, K. J. Hamill, Y. Wu, J. L. Eisenberg, S. Hiroyasu, J. C. R. Jones, *Adv. Wound Care* **2014**, *3*, 247.
[3] D. Tsuruta, T. Hashimoto, K. J. Hamill, J. C. Jones, *J. Dermatol. Sci.* **2011**, *62*, 1.
[4] L. Borradori, A. Sonnenberg, *J. Invest. Dermatol.* **1999**, *112*, 411.
[5] W. G. Carter, E. A. Wayner, T. S. Bouchard, P. Kaur, *J. Cell Biol.* **1990**, *110*, 1387.
[6] C. S. Chen, J. Tan, J. Tien, *Annu. Rev. Biomed. Eng.* **2004**, *6*, 275.
[7] S. H. M. Litjens, J. M. de Pereda, A. Sonnenberg, *Trends Cell Biol.* **2006**, *16*, 376.
[8] Q. Liu, S. Zheng, K. Ye, J. He, Y. Shen, S. Cui, J. Huang, Y. Gu, J. Ding, *Biomaterials* **2020**, *263*, 120327.
[9] C. Wu, *Cell Adhes. Migr.* **2007**, *1*, 13.
[10] M. S. Bauer, F. Baumann, C. Daday, P. Redondo, E. Durner, M. A. Jobst, L. F. Milles, D. Mercadante, D. A. Pippig, H. E. Gaub, *Proc. Natl. Acad. Sci. USA* **2019**, *116*, 6766.
[11] P. W. Oakes, M. L. Gardel, *Curr. Opin. Cell Biol.* **2014**, *30*, 68.
[12] E. A. Cavalcanti-Adam, T. Volberg, A. Micoulet, H. Kessler, B. Geiger, J. P. Spatz, *Biophys. J.* **2007**, *92*, 2964.
[13] J. Malmström, B. Christensen, H. P. Jakobsen, J. Lovmand, R. Foldbjerg, E. S. Sørensen, D. S. Sutherland, *Nano Lett.* **2010**, *10*, 686.
[14] M. Arnold, E. A. Cavalcanti-Adam, R. Glass, J. Blümmel, W. Eck, M. Kantlehner, H. Kessler, J. P. Spatz, *ChemPhysChem* **2004**, *5*, 383.
[15] X. Yao, R. Peng, J. Ding, *Adv. Mater.* **2013**, *25*, 5257.
[16] S. Zheng, Q. Liu, J. He, X. Wang, K. Ye, X. Wang, C. Yan, P. Liu, J. Ding, *Nano Res.* **2022**, *15*, 1623.
[17] J. E. Gautrot, J. Malmström, M. Sundh, C. Margadant, A. Sonnenberg, D. S. Sutherland, *Nano Lett.* **2014**, *14*, 3945.
[18] A. Pora, S. Yoon, R. Windoffer, R. E. Leube, *J. Invest. Dermatol.* **2019**, *139*, 1876.
[19] W. Wang, A. Zuidema, L. Te Molder, L. Nahidiazar, L. Hoekman, T. Schmidt, S. Coppola, A. Sonnenberg, *J. Cell Biol.* **2020**, *219*, e201904137.
[20] A. C. Laly, K. Sliogeryte, O. J. Pundel, R. Ross, M. C. Keeling, D. Avisetti, A. Waseem, N. Gavara, J. T. Connelly, *Sci. Adv.* **2021**, *7*, eabd6187.
[21] D. Tsuruta, S. B. Hopkinson, J. C. Jones, *Cell Motil. Cytoskeleton* **2003**, *54*, 122.
[22] L. Nahidiazar, M. Kreft, B. van den Broek, P. Secades, E. M. Manders, A. Sonnenberg, K. Jalink, *J. Cell Sci.* **2015**, *128*, 3714.
[23] H. Fredriksson, Y. Alaverdyan, A. Dmitriev, C. Langhammer, D. S. Sutherland, M. Zäch, B. Kasemo, *Adv. Mater.* **2007**, *19*, 4297.
[24] R. Michel, I. Reviakine, D. Sutherland, C. Fokas, G. Csucs, G. Danuser, N. D. Spencer, M. Textor, *Langmuir* **2002**, *18*, 8580.
[25] G. L. Kenausis, J. Vörös, D. L. Elbert, N. Huang, R. Hofer, L. Ruiz-Taylor, M. Textor, J. A. Hubbell, N. D. Spencer, *J. Phys. Chem. B* **2000**, *104*, 3298.
[26] R. Michel, J. W. Lussi, G. Csucs, I. Reviakine, G. Danuser, B. Ketterer, J. A. Hubbell, M. Textor, N. D. Spencer, *Langmuir* **2002**, *18*, 3281.
[27] H. Agheli, J. Malmström, E. Larsson, M. Textor, D. S. Sutherland, *Nano Lett.* **2006**, *6*, 1165.
[28] N.-P. Huang, R. Michel, J. Voros, M. Textor, R. Hofer, A. Rossi, D. L. Elbert, J. A. Hubbell, N. D. Spencer, *Langmuir* **2001**, *17*, 489.
[29] J. Schnitzbauer, M. T. Strauss, T. Schlichthaerle, F. Schueder, R. Jungmann, *Nat. Protoc.* **2017**, *12*, 1198.
[30] S. H. Kristensen, G. A. Pedersen, R. Ogaki, V. Bochenkov, L. N. Nejsum, D. S. Sutherland, *Acta Biomater.* **2013**, *9*, 6158.
[31] J. Malmström, J. Lovmand, S. Kristensen, M. Sundh, M. Duch, D. S. Sutherland, *Nano Lett.* **2011**, *11*, 2264.
[32] G. Walko, M. J. Castañón, G. Wiche, *Cell Tissue Res.* **2015**, *360*, 363.
[33] R. Kalluri, M. Zeisberg, *Nat. Rev. Cancer* **2006**, *6*, 392.
[34] B. Coulomb, C. Lebreton, L. Dubertret, *J. Invest. Dermatol.* **1989**, *92*, 122.
[35] L. Koivisto, K. Larjava, L. Häkkinen, V.-J. Uitto, J. Heino, H. Larjava, *Cell Adhes. Commun.* **1999**, *7*, 245.
[36] B. Yue, *J. Glaucoma* **2014**, *23*, S20.
[37] S. H. Kristensen, G. A. Pedersen, L. N. Nejsum, D. S. Sutherland, *Nano Lett.* **2012**, *12*, 2129.
[38] A. S. Andersen, H. Aslan, M. Dong, X. Jiang, D. S. Sutherland, *Nano Lett.* **2016**, *16*, 2114.
[39] E. Hintermann, M. Bilban, A. Sharabi, V. Quaranta, *J. Cell Biol.* **2001**, *153*, 465.
[40] R. Hofer, M. Textor, N. Spencer, *Langmuir* **2001**, *17*, 4014.
[41] J. W. Lussi, C. S. Tang, P.-A. Kuenzi, U. Staufer, G. Csucs, J. Vörös, G. Danuser, J. A. Hubbell, M. Textor, *Nanotechnology* **2005**, *16*, 1781.
[42] T. J. Collins, *BioTechniques* **2007**, *43*, 25.
[43] S. Strauss, R. Jungmann, *Nat. Methods* **2020**, *17*, 789.
[44] D. Nečas, P. Klapetek, *Open Phys.* **2012**, *10*, 181.